Langmuir Article

pubs.acs.org/Langmuir

Remarkable Photothermal Effect of Interband Excitation on Nanosecond Laser-Induced Reshaping and Size Reduction of Pseudospherical Gold Nanoparticles in Aqueous Solution

Daniel Werner,[†] Shuichi Hashimoto,*[,†] and Takayuki Uwada[‡]

[†]*Department of Ecosystem Engineering, The University of Tokushima, Tokushima 770-8506, Japan, and* [‡]*Department of Applied Chemistry and Institute of Molecular Science, National Chiao Tung University, Hsinchu 30010, Taiwan*

Received January 3, 2010. Revised Manuscript Received February 27, 2010

An in situ spectroscopic study of the nanosecond laser-induced melting and size reduction of pseudospherical gold nanoparticles with 54 ± 7 nm diameter allowed the observation of a heating efficiency that was very dependent on the excitation wavelength. A remarkably greater efficiency was observed for the photothermal effect of interband excitation than that of intraband excitation. This noteworthy observation is ascribed to an altered electron heat capacity, c_e, during photoexcitation depending on the excitation energy, which is a phenomenon that has not been realized previously. As a result, a 60% reduction of the specific heat capacity, c_p, compared to that of bulk gold was obtained for interband excitation at 266 nm whereas the c_p value for the excitation of the intraband transition at 532 nm was unaltered. A semiquantitative explanation was given for this striking phenomenon induced by interband excitation in which excitation−relaxation cycles of electrons upon excitation of 5d electrons to the 6sp band lead to a reduced number of electrons contributing to the electron temperature rise in the vicinity of the Fermi level during the nanosecond laser pulse duration. By contrast, electronic excitation within the 6sp band results in no net reduction in the number of electrons near the Fermi level, giving rise to a value of c_p similar to that of bulk gold. Our finding that the heat capacity of gold nanoparticles can be changed upon UV laser excitation is important for understanding the fundamental nature of noble metal nanoparticles. Furthermore, this finding might be useful for preparing new metal alloy particles as well as for manipulating the thermodynamic properties of the nanoparticles.

Introduction

The interaction of metal nanoparticles with light brings about fascinating optical phenomena such as the plasmonic enhancement of the electromagnetic field,[1,2] nonlinear optical responses,[3,4] and photothermal effects[5,6] and thus attracted a great deal of attention in the past decade. In particular, gold and silver nanoparticles (NPs) have played a central role in these fields because of their remarkable electronic and optical properties that are distinct from their bulk counterparts,[7] which may find applications in catalysis,[8,9] bioconjugation,[10,11] nanomedecine,[12,13] and miniaturized photonic devices.[14] In these applications, an important role played by lasers is worth mentioning because they carry advantageous features such as high photon densities, distinct photon energies, various pulse widths from femtosecond to nanosecond time durations, and tunable polarization properties that permit the precise control of excitation. Therefore, the fundamental aspect of interplay between NPs and lasers is critical to understanding how photon energies are utilized by NPs to realize desired functions to the maximum extent.

One example seeking such a direction is a study on laser-induced size reduction in which the exposure of Au and Ag NPs to a single shot or a number of shots allowed the size reduction or fragmentation.[15−21] The method acquired solid recognition as a convenient, swift technique for preparing particles profoundly smaller than the original ones as opposed to conventional chemical techniques where a time-consuming oxidative etching process has to be carried out separately for the size reduction. Koda and co-workers[15] were the first to propose a heating−melting−evaporation concept for the observation of the size reduction of chemically prepared aqueous Au NPs with sizes ranging from 19 to 47 nm diameter by exposure of the surface plasmon band to various intensities and numbers of a 532 nm nanosecond pulsed-laser beam. In support of Koda's photothermal mechanism, Inasawa and co-workers[16] conducted further

*Corresponding author. E-mail: hashi@eco.tokushima-u.ac.jp.

(1) Bohren, C. F. *Am. J. Phys*. **1983**, *51*, 323.
(2) Eustis, S.; El-Sayed, M. A. *Chem. Soc. Rev*. **2006**, *35*, 209.
(3) Kityk, I. V.; Ebothe, J.; Fuks-Janczarek, I.; Umar, A. A.; Kobayashi, K.; Oyama, M.; Sahraoui, B. *Nanotechnology* **2005**, *16*, 1687.
(4) Debrus, S.; Lafait, J.; May, M.; Pincon, N.; Prot, D.; Sella, C.; Venturini, J. *J. Appl. Phys*. **2000**, *88*, 4469.
(5) Lefullin, R. R.; Joenathan, C.; George, T. F.; Zharov, V. P. *Nanomedicine* **2006**, *1*, 473.
(6) Pustovalov, V. K.; Smetannikov, A. S.; Zharov, V. P. *Laser. Phys. Lett*. **2008**, *5*, 775.
(7) Kreibig, U.; Vollmer, M. *Optical Properties of Metal Clusters*; Springer: Berlin, 1995.
(8) Haruta, M. *Catal. Today* **1997**, *36*, 153–166.
(9) Bond, G. C.; Thompson, D. T. *Catal. Rev*. **1999**, *41*, 319–388.
(10) Copland, J. A.; Eghtedari, M.; Popov, V. L.; Kotov, N.; Mamedova, N.; Motamedi, M.; Oraevsky, A. A. *Mol. Imaging Biol*. **2004**, *6*, 341.
(11) Petersen, S.; Barcicowski, S. *Adv. Mater*. **2009**, *19*, 1167.
(12) Huang, X.; Jain, P. K.; El-Sayed, I. H.; El-Sayed, M. A. *Nanomedicine* **2007**, *2*, 681.
(13) Shukla, R.; Bansal, V.; Chaudhary, M.; Basu, A.; Bhonde, R. R.; Sastry, M. *Langmuir* **2005**, *21*, 10644.
(14) Maier, S. A. *Curr. Nanosci*. **2005**, *1*, 17–22.
(15) Takami, A.; Kurita, H.; Koda, S. *J. Phys. Chem. B* **1999**, *103*, 1226.
(16) Inasawa, S.; Sugiyama, M.; Yamaguchi, Y. *J. Phys Chem. B* **2005**, *109*, 9404.
(17) Pyatenko, A.; Yamaguchi, M.; Suzuki, M. *J. Phys. Chem. C* **2009**, *113*, 9078.
(18) Yamada, K.; Tokumoto, Y.; Nagata, T.; Mafune, F. *J. Phys. Chem. B* **2006**, *110*, 11751.
(19) Yamada, K.; Miyajima, K.; Mafune, F. *J. Phys. Chem. C* **2007**, *111*, 11246.
(20) Shoji, M.; Miyajima, K.; Mafune, F. *J. Phys. Chem. C* **2008**, *112*, 1929.
(21) Muto, H.; Miyajima, K.; Mafune, F. *J. Phys. Chem. C* **2008**, *112*, 5810.

detailed research through the use of a 355 nm picosecond laser and revealed that the size reduction of Au NPs takes place by a layer-by-layer mechanism based on the observation of a bimodal distribution of particle sizes that are slightly smaller and much smaller than the original ones. They concluded that irradiation by the picosecond laser pulses is the most efficient way to induce the size reduction of gold NPs over femtosecond or nanosecond pulses. Later, Pyatenko[17] made a calculation to examine the melting and size reduction of gold NPs and concluded that the photothermal mechanism prevails at low laser intensities. He also drew a conclusion that the excitation of the surface plasmon band of gold by a nanosecond laser at 532 nm is more efficient because of a greater absorption cross section, C_{abs}, compared with those at other wavelenghths such as 1064 and 355 nm but gave no experimental proof.

Previous size reduction studies have mostly been carried out at only one excitation wavelength, and no comparison was made with the effect of the excitation laser wavelength on size reduction, focusing on the difference in inter- and intraband transitions, for instance. To begin, the dielectric function of gold ($\varepsilon(\omega)$) is described by a combination of an interband term ($\varepsilon_{IB}(\omega)$) that accounts for the response of 5d electrons to a 6sp conduction band and a Drude term ($\varepsilon_D(\omega)$) due to free conduction electrons; thus $\varepsilon(\omega) = \varepsilon_{IB}(\omega) + \varepsilon_D(\omega)$.[7] The localized surface plasmon resonance representing the optical properties characteristic of gold NPs originates from the latter term (i.e., photoexcitation of the free electrons). A collective oscillation of photoexcited free electrons on the surface of Au NPs takes place through the interaction with the electromagnetic field of light and exhibits a resonance frequency in the visible region. For instance, the extinction spectrum of gold NPs of 10 nm diameter dispersed in water exhibits a distinct resonance peak at approximately 520 nm, and the peak position and intensity undergo changes depending sensitively on the particle size and shape.[7] By contrast, the interband transition is insensitive to the particle size and shape but gives at least two broad absorption bands at 330 and 470 nm.[7] As a corollary, we anticipated that not only the light absorption cross section but also the electron dynamics and subsequent thermal relaxation process initiated by photoexcitation should be strongly affected by the excitation wavelength. However, this wavelength-dependent laser-induced melting and size reduction of gold NPs are not fully understood despite accumulated knowledge from laser ablation studies carried out in the past. For instance, Mafune and co-workers[18−21] demonstrated that the excitation of the interband transition by a 355 nm nanosecond laser can induce the severe fragmentation of gold NPs because of the Coulombic explosion mechanism. Nevertheless, it is still not clear whether their observation purely originates from the effect of the interband excitation because they applied laser powers such as 0.5−25 $J \cdot cm^{-2}$ far exceeding the laser ablation threshold (i.e., energies high enough to bring about high temperatures well over the boiling point of bulk gold). This makes it difficult to determine the morphological changes near the laser ablation threshold. In addition, particles employed in previous research are more or less polydisperse, which precludes precise spectroscopic studies besides TEM measurements. Furthermore, it should be pointed out that the particle size is an important factor affecting both heat dissipation and the contribution of the interband transition relative to the intraband one depending on the excitation wavelength: if the particle is smaller than 20 nm in diameter, for instance, the contribution of the plasmon band is considerably large even for excitation at 355 nm. Such a consideration was lacking in the past.

In the present study, we carried out in situ extinction spectroscopic and TEM investigations[22] of the nanosecond laser-induced size reduction of Au NPs by seriously considering the critical issues paid less attention to previously. We employed the lowest possible laser intensities that can avoid the generation of excess heat, giving rise to the explosive evaporation of NPs.[23,24] As for the excitation wavelength, we used three laser wavelengths, 266, 355, and 532 nm. The former two have energies appropriate for promoting the interband transition, and the latter corresponds to the energy of the intraband transition. Notably, we employed pseudospherical particles with a narrow size distribution. This is important in eliminating the effect of inhomogeneous spectral broadening due to polydispersity. Besides that, the narrow size distribution guarantees the feasible estimation of absorbed energies by the particles at each excitation wavelength on the basis of Mie theory calculations.[25] Given that the absorbed energy is directly related to the temperature rise, a precise evaluation of absorbed energy at various wavelengths is important in assessing how efficiently the absorbed energy is converted into heat, resulting in melting and size reduction.

In spite of our simple experimental approach, we made an important finding that the heat capacity of gold NPs during photoexcitation can be reduced by nanosecond pulsed-laser heating through the interband excitation. This remarkable heat capacity change of gold NPs is relevant to a fundamental thermodynamic property that has not been observed experimentally, although some theoretical prediction has been made previously.[26] Moreover, our finding may open up a laser-based preparation of new metal alloys by choosing the proper excitation laser wavelengths for the materials.

Experimental Section

Aqueous solutions of gold NPs with nominal diameters of 20 nm (cat. no. EMGC20) and 60 nm (cat. no. EMGC60) were purchased from British Biocell International (Cardif, U.K.). These particles were synthesized using a variation of the Frens's citrate reduction method.[27] The particle size determined presently by the observation of TEM images is 19 ± 3 for EMGC20 and 54 ± 7 for EMGC60 (Supporting Information A). We tentatively refer to these particles as 20 and 55 nm Au NPs for convenience.

The laser irradiation of 2.0 mL aliquots of Au NP aqueous solutions contained in a quartz cuvette ($10 \times 10\ mm^2$) was carried out with the unfocused beam of the second, third, and fourth harmonics of a Nd:YAG laser (Continuum, Surelite I-10; repetition rate, 10 Hz; pulse width, 4−6 ns). The beam diameter was measured to be 8 mm for 532 nm, 7 mm for 355 nm, and 6 mm for 266 nm. The solutions were magnetically stirred during the irradiation. A 150 W short-arc Xe lamp (Hamamatsu, L2274) was used as a monitor light for in situ spectroscopic measurements in which the light extinction (absorption and scattering) signals were detected by a multichannel spectrophotometer (StellaNet, BlueWave). Steady-state extinction spectra of NP solutions were recorded on a UV−vis spectrophotometer (Hitachi, H-2010). Transmission electron micrographs (TEM) of the particles were obtained with a Hitachi H-800 operated at 200 kV.

(22) Werner, D.; Hashimoto, S.; Tomita, T.; Matsuo, S.; Makita, Y. *J. Phys. Chem. C* **2008**, *112*, 16801.
(23) Yamada, K.; Itoh, T.; Tsuboi, Y. *Appl. Phys. Express* **2008**, *1*, 087001.
(24) Hashimoto, S.; Uwada, T.; Hagiri, M.; Takai, H.; Ueki, T. *J. Phys. Chem. C* **2009**, *113*, 20640.
(25) Bohren, C. F.; Huffman, D. R. *Absorption and Scattering of Light by Small Particles*; Wiley: New York, 1983.
(26) Hopkins, P. E. *J. Heat Trans.* **2010**, *132*, 014504.
(27) Frens, G. *Nat. Phys. Sci.* **1973**, *241*, 20.

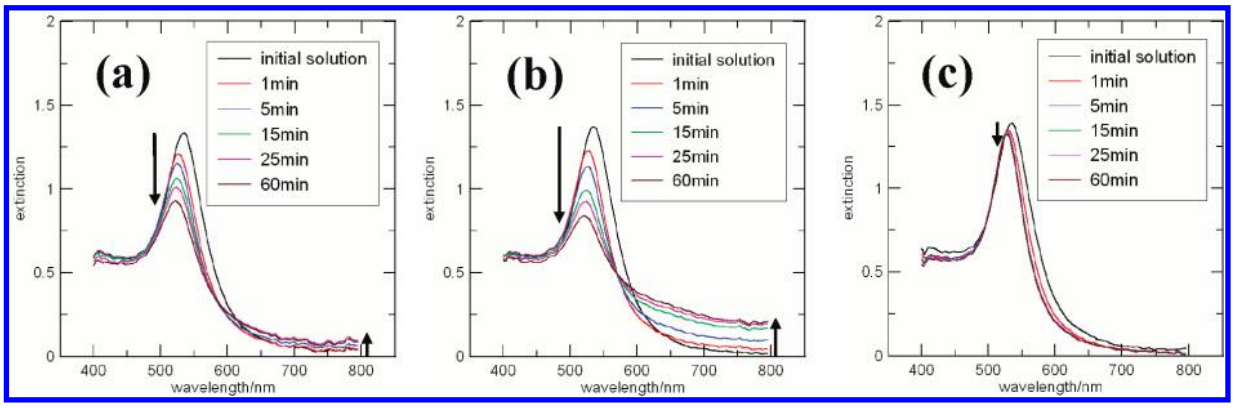

Figure 1. In situ extinction spectra of initial 55 nm gold particles in aqueous solution on excitation at various wavelengths with virtually the same absorbed energy of 300 J g^{-1}: (a) λ_{ex} = 266 nm (10.3 ± 1.3 mJ cm^{-2} fluence), (b) λ_{ex} = 355 nm (11.2 ± 0.9 mJ cm^{-2} fluence), and (c) λ_{ex} = 532 nm (6.0 ± 0.4 mJ cm^{-2} fluence). The arrows show the direction of spectral changes with increasing irradiation period.

Results

As a measure of the absorbed energy by a unit mass of gold upon irradiation of a single shot of a pulsed laser, we employ Q (J g^{-1} $pulse^{-1}$) given by eq 1 because this quantity is independent of the particle size and excitation wavelength.

$$Q = \frac{C_{abs}^{\lambda} P}{\rho V} \quad (1)$$

where C_{abs}^{λ} (m^2) is the absorption cross section of a single Au NP at a given excitation wavelength, P (J m^{-2} $pulse^{-1}$) is the laser fluence, ρ (g m^{-3}) is the density of gold, and V (m^3) is the volume of a gold NP. (See Supporting Information B for another method of estimation.) The absorption cross section at each wavelength was calculated on the basis of the Mie theory.[25] The extinction spectra thus obtained were in good agreement with those measured on the spectrophotometer for 55 and 20 nm gold spheres (Supporting Information Figures S1 and S2). Traditionally, the absorbed laser energy was directly related to the melting and evaporation thresholds defined by eqs 2a and 2b under the condition that the heat losses due to both thermal conduction/convection and blackbody radiation are negligible:[15−17,28−31]

$$Q_{melt} = c_p^s(T)[T_{melt} - T_0] \quad (2a)$$

$$Q_{evap} = c_p^s(T)[T_{melt} - T_0] + \Delta H_{melt} + c_p^l[T_{evap} - T_{melt}] \quad (2b)$$

where c_p represents the specific heat capacity under atmospheric pressure, T_{melt} stands for the melting point of gold, and T_{evap} is the boiling point, the values of which were taken from those of bulk gold.[32] Superscripts s and l of c_p denote the solid and liquid phases, respectively.

Figure 1 shows the in situ extinction spectra of 55 nm gold particles in aqueous solution on exposure to (a) 266, (b) 355, and (c) 532 nm laser beams at the absorbed energy, Q, of 300 J g^{-1} $pulse^{-1}$.

A spectral band with a peak at 535 nm originating from Au NPs is ascribed to the surface plasmon resonance band, the peak position and intensity of which strongly depend on the particle diameter as well as the dielectric function of the medium.[7] Accordingly, the high monodispersity of the NPs permits the peak position and intensity of the surface plasmon band to serve as a measure of the particle size.[33] A remarkable reduction was observed in the intensity of the plasmon band on continuous irradiation by the 266 and 355 nm lasers. For instance, the amount of reduction in the extinction peak values of $\Delta A^{266\ nm} = -0.412$ and $\Delta A^{355\ nm} = -0.53$ was obtained after 60 min of irradiation, accompanied by an appreciable blue shift of 15 nm from 535 to 520 nm. Additionally, an increased contribution in the extinction spectrum in the 600−800 nm region was observed for two reasons. First, a continuous size reduction due to irradiation under a constant atomic concentration of Au results in an increased number of small particles contributing to the increased extinction in the red region. A spectral simulation can reproduce the spectral changes observed in Figure 1 (Supporting Information C). Second, the coagulation and coalescence of small NPs to form "snake-like" structures is also responsible as revealed by the TEM images given below. In contrast, the irradiation at 532 nm exhibited only a slight decrease in intensity ($\Delta A_{532\ nm} = -0.071$) and a small blue shift of 6 nm in the plasmon band after 15 min of irradiation; further irradiation to 60 min gave practically no remarkable spectral changes. In situ spectral changes at various Q and λ_{ex} values are given in Supporting Information D.

Figure 2 shows the decrease in the peak intensity of the plasmon band, ΔA, as a function of absorbed energy, Q, after 60 min of laser irradiation at 266, 355, and 532 nm. This Figure gives the entire picture of the size and shape changes that are dependent on both Q and the excitation wavelengths employed in this study.

The data points for each wavelength exhibit two-step threshold behavior. The first step is located in a range from $\Delta A = -0.05$ to -0.2 where only small intensity reductions and slight blue shifts of the plasmon band are discernible as typically shown as a spectrum in Figure 1c. Corresponding TEM images given in Figure 3 show appreciable reshaping from the initial faceted (Figure 3a1,b1,c1) to spherical appearance (Figure 3a2, b2, c2) due to surface melting with no recognizable size changes.

The second step corresponding to data points carrying ΔA between −0.4 and −0.7 indicates large spectral modifications in

(28) Link, S.; Burda, C.; Nikoobakht, B.; El-Sayed, M. A. *J. Phys. Chem. B* **2000**, *104*, 6152.
(29) Hartland, G. V.; Hu, M.; Sader, J. E. *J. Phys. Chem. B* **2003**, *107*, 7472.
(30) Agurre, C. M.; Moran, C. E.; Young, J. F.; Halas, N. J. *J. Phys. Chem. B* **2004**, *108*, 7040.
(31) Besner, S.; Kabashin, A. V.; Winnik, F. M.; Meunier, M. *J. Phys. Chem. C* **2009**, *113*, 9526.
(32) Green, D. W.; Perry, R. H. *Perry's Chemical Engineers' Handbook*, 8th ed.; McGraw-Hill: New York, 2007; pp 2−158.
(33) Njoki, P. N.; Lim, I. S.; Mott, D.; Park, H.-Y.; Khan, B.; Mishra, S.; Sujakumar, R.; Luo, J.; Zhong, C.-J. *J. Phys. Chem. C* **2007**, *111*, 14664.

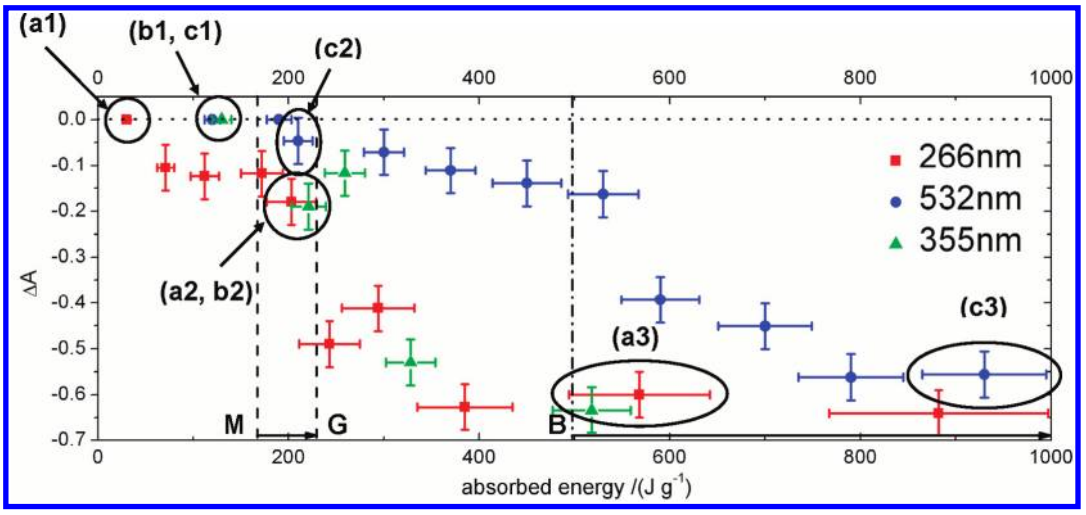

Figure 2. Difference peak extinction value (ΔA) of the plasmon band as a function of the absorbed energy for the initial 55 nm gold particle in aqueous solution as a function of excitation wavelengths of 266, 355, and 532 nm. The data points represent the values for an irradiation period of 60 min (10 Hz, 36 000 laser shots). The dotted line (M) on the far left represents the absorbed energy corresponding to the melting point of bulk gold calculated with eq 2a, and the second dotted line (G) shows the energy at which the melting enthalpy (ΔH_{melt} = 62.8 J g^{-1}) is consumed. The dashed-dotted line (B) on the far right shows the energy where the boiling point of bulk gold calculated with eq 2b is reached. The data points marked with circles show the TEM images that are given in Figure 3.

terms of remarkable reductions and blue shifts in the plasmon band, similar to the spectral changes observed in Figure 1a,b. TEM observations of these samples revealed the marked size reduction of initial 54 ± 7 nm to an average of 6 nm particles (Figure 3a3,a3-1,c3). Notably, "snakelike" fused structures of smaller particles were obtained, suggesting a size reduction caused by evaporation due to high temperature.

An inspection of the TEM image of the original 55 nm particles upon excitation with 266 nm laser light (Figure 3a series) at relatively high absorbed energy Q of 568 J g^{-1} pulse^{-1} reveals that the particles were gradually reduced in size while generating much smaller particles with an average size of 7 nm, resulting in a bimodal size distribution. Bimodal distributions similar to this were also obtained for excitations at 355 and 532 nm. Note here that at absorbed energies of Q, where no spectral changes could be observed, the shapes and sizes of the NPs remain unchanged (Figure 3a1, b1, c1) because the melting point of gold could not be reached. One should keep in mind that the present experiments were carried out under the condition of low laser intensities that preclude violent mechanisms such as the explosive evaporation due to extremely high temperatures[23,24] and the Coulombic explosion arising from multiply ionized states[18−21] caused by the photoionization or thermionic emission of electrons. (See Supporting Information E for justification.) Consistent with this assumption, we observed no explosion-like phenomena in the TEM images but only a gradual size reduction by the emission of very small particles, reminiscent of the layer-by-layer size reduction concept proposed by Inasawa.[16] Note here that the bimodal distribution does not indicate the original faceted particles accompanied by fragmented particles but rather the size-reduced spherical particles along with much smaller daughter particles.

A comparison of the energy thresholds for each wavelength in Figure 2 reveals that absorbed energies, Q, required to initiate the melting for reshaping and evaporation leading to a gradual size reduction by the 532 nm laser are approximately 2 to 3 times greater than the energies of the 266 and 355 nm lasers. To analyze the remarkably different behavior of ΔA versus Q curves dependent on λ_{ex}, the melting and evaporation thresholds, Q_{melt} and Q_{evap}, were calculated for the simple heating of a 55 nm gold particle based upon eqs 2a and 2b using the c_p values of bulk gold

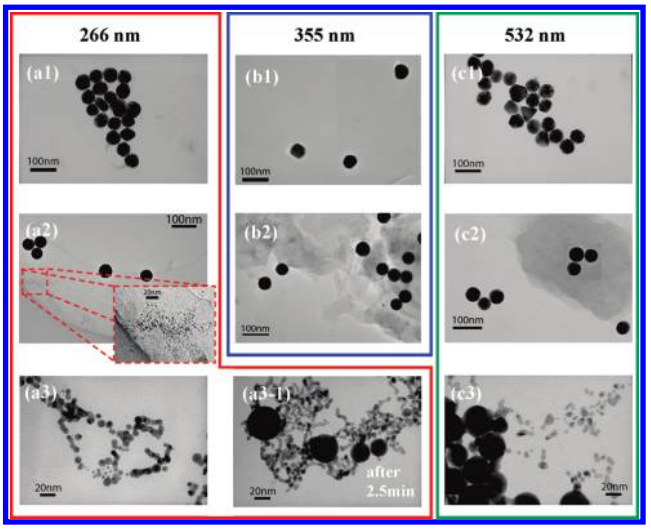

Figure 3. TEM images of initial 55 nm gold particles after 60 min of laser irradiation (10 Hz, 36 000 shots) at wavelengths of (a) 266, (b) 355, and (c) 532 nm. The notation of a number next to a letter is related to the data points given in Figure 2: 1 indicates gold nanoparticles with no shape and size changes, 2 indicates reshaping, and 3 indicates the evaporation of the initial gold NPs in solution. Only image a3-1 was taken for an irradiation period of 2.5 min to show clearly the occurrence of the bimodal distribution.

and included in Figure 2, assuming an initial temperature, T_0, of 298 K. The dotted line (M) on the far left in Figure 2 represents Q_{melt}, and the second dotted line (G) shows the energy at which the particle is assumed to undergo whole melting as a result of the consumption of the melting enthalpy (ΔH_{melt} = 62.8 J g^{-1}). The dashed-dotted line (B) on the far right shows the energy, Q_{evap}, where the boiling point of bulk gold is reached. Importantly, when excited at 532 nm, the energies corresponding to lines H and Z are in close agreement with the experimental values of Q_{melt} and Q_{evap} for the laser heating of a 55 nm gold NP, suggesting that the 55 nm gold NP has melting and evaporation behavior that is quite similar to that of bulk gold. On the contrary, the Au particle undergoes melting and evaporation at much lower laser energies when excited at 266 and 355 nm.

The temperature rise can be estimated for a single Au NP by dividing Q by the specific heat capacity under the assumption of negligible heat losses. Besides, we assume that our 55 nm gold particles can still be treated as bulk gold with respect to the melting point (1337 K) because melting point depression due to the curvature effect of small particles is remarkable only for diameters below 15 nm.[34−37] The specific heat capacity in the solid phase of bulk gold is slightly temperature-dependent, whereas that in the liquid state is constant.[32] Here, we estimate the heat capacity in the liquid phase, c_p^{l}, for two wavelengths (532 and 266 nm) on the basis of experimentally determined $Q_\lambda^{\mathrm{evap}}$ and $Q_\lambda^{\mathrm{melt}}$ with bulk values of ΔH_{melt}, T_{eavp}, and T_{melt} by eq 3

$$c_p^{\mathrm{l}}(\lambda) = \frac{(Q_\lambda^{\mathrm{evap}} - Q_\lambda^{\mathrm{melt}} - \Delta H_{\mathrm{melt}})}{(T_{\mathrm{evap}} - T_{\mathrm{melt}})} \tag{3}$$

which yields c_p^{l}(532 nm) = (0.16 ± 0.02) J g^{-1} K^{-1} and c_p^{l}(266 nm) = (0.06 ± 0.01) J g^{-1} K^{-1}. (See Supporting Information F for details.) The heat capacity calculated for 532 nm excitation, c_p^{l}(532 nm), is in good agreement with that of bulk gold (c_p^{l} = 0.149 J g^{-1} K^{-1}.[32] Note that we neglected heat losses through heat dissipation[38−40] and a disturbance by the scattered light of cavity formation[41−43] surrounding the irradiated NPs for the evaluation of c_p^{l}. The striking result is that the specific heat capacity estimated for the excitation at 266 nm is 60% smaller than that of bulk gold. We also experimentally evaluated the solid-phase specific heat capacities, c_p^{s}(532 nm) = (0.19 ± 0.03) J g^{-1} K^{-1} and c_p^{s}(266 nm) = (0.05 ± 0.02) J g^{-1} K^{-1}) from the onsets of melting, although the value of c_p^{s}(266 nm) is not very accurate because of difficulty in determining the exact value of Q_{melt}. Here, the average c_p^{s} value for bulk gold between room temperature and the melting point is known to be 0.144 J g^{-1} K^{-1}.[32] Thus, the value of c_p^{s} is significantly smaller for the excitation at 266 nm than that for the excitation at 532 nm, which is in accordance with the excitation-wavelength-dependent values of c_p^{l} that we obtained.

We also carried out the in situ spectroscopic measurements for 20 nm gold particles in order to gain insight into the size-dependent melting and size reduction that have not been attempted previously (Supporting Information G). The excitation-wavelength-dependent melting and size reduction reminiscent of 55 nm particles was observed (Supporting Information H). For 20 nm Au particles, however, we failed to estimate the values of the specific heat capacities, c_p^{l} and c_p^{s}, because of appreciable heat losses observed for the small particles.

Discussion

It follows from our result that the excitation of the interband transition of Au NPs by nanosecond 266 and 355 nm lasers results in a pronounced reduction in the specific heat capacity, leading to the very efficient size reduction, distinct from the result of excitation at 532 nm when compared at virtually the same absorbed laser energy, Q. The prototypical example of such experiments was given in Figure 1, and the exhaustive collection of data was depicted in Figure 2. Until now, no attempts have been made to observe the size reduction comparing the interband excitation with intraband excitation. Here we show a semiquantitative picture of the electronic relaxation process characteristic of the excitation wavelength, giving rise to the modified heat capacity, c_p. Most importantly, the bulk c_p value has been intuitively assumed previously in dealing with the photothermal mechanism of the laser-induced size reduction of Au and Ag NPs.[14−16] This may not necessarily be valid.

The electron heat capacity, c_e, in metals is described by eq 4a,[44]

$$c_e = \int_0^\infty (E - E_F)\frac{\mathrm{d}f(E, T_e)}{\mathrm{d}T_e} D(E)\,\mathrm{d}E \tag{4a}$$

where E_F stands for the Fermi energy, $f(E, T_e)$ represents the Fermi distribution at energy E and electron temperature T_e, and $D(E)$ is the density of states (DOS). At low electron temperatures of $k_B T_e \ll E_F$ (where k_B is the Boltzmann constant), which are applicable to our experimental T_e estimated for a long pulse duration of ~5 ns, the change in the Fermi distribution occurs only near the Fermi energy. Then the solution for the free electron gas of a metal at thermal equilibrium leads to the well-established equation[44]

$$c_e \cong \gamma T_e \text{ in which } \gamma = \frac{1}{3}\pi^2 D(E_F) {k_B}^2 \tag{4b}$$

Here, $D(E_F)$ denotes the DOS at the Fermi level, which is defined by $D(E_F) = 3N/2E_F$, with N being the concentration of electrons at the Fermi level. The significance of eq 4b is that c_e is proportional to N of the degenerated electron gas and increases linearly with T_e.

The electronic excitation of gold NPs is divided into two categories: the intraband (within the 6sp band) and interband (5d to 6sp) excitations. The intraband transition of conduction electrons occurs because of the excitation of the surface plasmon resonance band in the visible region whereas the interband transition takes place mainly in the UV region. The onset of the interband transition occurs at about 2.4 eV (518 nm) with a tail at 1.8 eV (689 nm) for bulk gold at room temperature[45] (Supporting Information I). After nanosecond pulsed-laser irradiation, Au NPs are heated to a maximum temperature of 3129 K, the evaporation point of gold, where the Fermi edge is smeared out with an energy range of $2k_B T_e$ = 0.54 eV at thermal equilibrium (Supporting Information I, Figure S11). The lowest energy to promote electrons from the 5d band to the 6sp band below the Fermi energy is 1.6 eV ($L_{6+5}{}^{+} - L_4{}^{-}$ transition), which was derived from the relativistic band structure calculation.[46,47] Note here that an additional 0.8 eV should be included to reach the Fermi level.[46,47] This means that at least the photon energy of 2.4 eV is required for the excitation of electrons from the 5d to the 6sp band to overcome the interband transition threshold. At 3129 K, electrons within the energy interval of 0.54 eV are brought to energy levels above the Fermi level at thermal equilibrium, which generates holes below the Fermi energy. Hence, the interband transition onset is reduced to 1.86 eV at a minimum, and the photoexcitation of 5d electrons to the 6sp band at 532 nm (2.33 eV) is theoretically possible. Even though this is the case, the

(34) Couchman, P. R.; Jesser, W. A. *Nature* **1977**, *269*, 481.
(35) Buffat, P.; Borel, J.-P. *Phys. Rev. A* **1976**, *13*, 2287.
(36) Ercolessi, F.; Andreoni, W.; Tosatti, E. *Phys. Rev. Lett.* **1991**, *66*, 911.
(37) Nanda, K. K. *Appl. Phys. Lett.* **2005**, *87*, 021909.
(38) Hu, M.; Hartland, G. V. *J. Phys. Chem. B* **2002**, *106*, 7029.
(39) Plech, A.; Kotaidis, V.; Grésillon, S.; Dahmen, C.; von Plessen, G. *Phys. Rev. B* **2004**, *70*, 195423.
(40) Goldenberg, H.; Tranter, C. J. *Br. J. Appl. Phys.* **1952**, *3*, 296.
(41) Lukianova-Hleb, E. Y.; Lapotko, D. O. *Nano Lett.* **2009**, *9*, 2160.
(42) Lapotko, D. *Opt. Express* **2009**, *17*, 2538.
(43) Kotaidis, V.; Dahmen, C.; von Plessen, G.; Springer, F.; Plech, A. *J. Chem. Phys.* **2006**, *124*, 184702.
(44) Kittel, C. *Introduction to Solid States Physics*, 8th ed.; Wiley: New York, 2004.
(45) Berciaud, S.; Cognet, L.; Tamarat, P.; Lounis, B. *Nano Lett.* **2005**, *5*, 515.
(46) Christensen, N. E.; Seraphin, B. O. *Phys. Rev. B* **1971**, *4*, 3321.
(47) Fukutani, H. *J. Phys. Soc. Jpn.* **1971**, *30*, 399.

Scheme 1. Illustration of Electron Excitation−Relaxation Processes for (a) 6sp Intraband Excitation and (b) 5d to 6sp Interband Excitation[a]

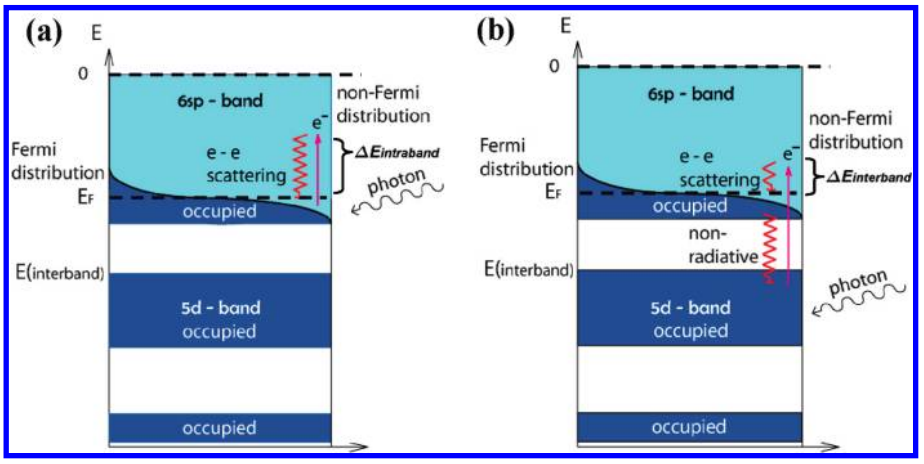

[a] Both processes initially generate a non-Fermi distribution followed by the formation of a Fermi distribution resulting from the electron−electron scattering.

interband absorption contributes only 5−20% of the total absorption cross section at temperatures below the evaporation point. This suggests that at the excitation wavelength of 532 nm the intraband transition is still dominant (Supporting Information I, Figure S10a). In contrast, excitation by UV light with λ = 266 and 355 nm allows the interband transition because their energies greatly exceed the interband separation. It is also the case that light with an energy surpassing the interband threshold can contribute to the excitation of the intraband transition; however, the absorption spectra of the intra- and interband transitions calculated for 60 nm Au NPs show that the contribution of the former in the UV region is minute (Supporting Information I, Figure S10a).

Scheme 1 illustrates the electron−electron thermalization process through the scattering of a single electron due to the intraband (a) and interband (b) transitions in a simplified band structure.

Here, photons of λ = 532 nm promote the conduction band electrons below the Fermi level to upper energy levels with an energy of $\Delta E_{\text{intraband}}$ = 2.33 eV at the maximum distance above the Fermi surface (Scheme 1a), temporarily resulting in a non-Fermi distribution. Then, followed by the electron−electron (e−e) scattering of excited electrons, the Fermi distribution with an electron temperature of T_e is reestablished after thermal equilibrium has been reached.

In contrast to the excitation at 532 nm, photons of λ = 355 and 266 nm have energies high enough to promote electrons from the 5d band to the 6sp band, a conduction band, of Au (Scheme 1b). As a result, the final energies of the electrons above the Fermi level are reduced by the interband separations of certain lower-lying band structures. For instance, 355 nm photons (3.49 eV) excite the $L_{6+5}^{+}-L_4^{-}$ (1.6 eV) transition[46,47] to the 6sp band below the Fermi energy, with 0.8 eV added to reach the Fermi level, and the $X_7^{+}-X_6^{-}$ (3.2 eV) transistion[46,47] above the Fermi surface with energies of $\Delta E_{\text{interband}}$ distributed from 0 to 1.16 eV. Likewise, the excitation by the 266 nm laser with a corresponding photon energy of 4.66 eV allows an interband transition of $X_7^{+}-X_6^{-}$ (3.2 eV) or $X_6^{+}-X_6^{-}$ (4.4 eV), leading to an energy ($\Delta E_{\text{interband}}$) of between 0 and 1.46 eV above the Fermi level.[46,47] Notably, the excitation in the plasmon band always gives higher energies above the Fermi level than that of the interband excitation ($\Delta E_{\text{interband}} < \Delta E_{\text{intraband}}$). For such electrons with energies of ΔE, interaction within the degenerated electron gas is well described by the Fermi liquid theory.[48−52] One of the consequences of the theory is that a single e−e scattering time τ_{e-e} for electrons with energy of ΔE at temperature T_e is described by

$$\tau_{e-e}^{-1} = K\frac{(\pi k_B T_e)^2 + (\Delta E)^2}{1 + e^{-\Delta E/(k_B T_e)}} \quad (5)$$

where K is given by $(m^*)^3/(8\pi^4\hbar^6)W_{e-e}$, with m^* being the electron effective mass and W_{e-e} being the angularly averaged scattering probability. For Au, K = 0.1 fs^{-1} eV^{-2}, which was estimated from femtosecond pump−probe spectroscopy.[52] Equation 5 dictates that an electron excited to the Fermi level (ΔE = 0) at T_e = 0 has an infinite lifetime because of no e−e scattering events as a result of the Pauli exclusion principle: all energy states below the Fermi level are occupied. On increasing ΔE, the lifetime or the e−e scattering time decreases rapidly in a parabolic manner. For $\Delta E \gg k_B T_e$, eq 5 can be reduced to

$$\tau_{e-e}^{-1} \approx K(\Delta E)^2 \quad (6)$$

This simple expression states that the e−e scattering rate constant (τ_{e-e}^{-1}) increases with increasing ΔE above the Fermi level. Thus, electrons excited to near the Fermi level suffer a longer scattering time or a longer period of e−e thermalization than those excited into higher levels. Burda et al.[53] revealed by their femtosecond pump−probe spectroscopy at an excitation wavelength of 800 nm (1.55 eV) that the electron thermalization time is on the order of < 500 fs, which is much longer than the time scale of the e−e scattering and e−h recombination events (10 fs) according to the Fermi liquid theory. They explained this long thermalization time on the basis of a picture in which all of the electrons interacting within the range of mutual influence undergo scattering with each other until they thermalize to the Fermi level.

(48) Ashcroft, N. W.; Mermin, N. D. *Solid State Physics*; Harcourt Brace: Orlando, FL, 1976.
(49) Fann, W. S.; Storz, R.; Tom, H. W. K.; Bokor, J. J. *Phys. Rev. B* **1992**, *46*, 13592.
(50) Schuttenmaer, C. A.; Aeschlimann, M.; Elsayed-Ali, H. E.; Miller, R. J. D.; Mantell, D. A.; Cao, J.; Cao, Y. *Phys. Rev. B* **1994**, *50*, 8957.
(51) Hertel, T.; Knoesel, E.; Wolf, M.; Ertl, G. *Phys. Rev. Lett.* **1996**, *76*, 535.
(52) Groeneveld, R. H. M.; Sprik, R.; Lagendijk, A. *Phys. Rev. B* **1995**, *51*, 11433.
(53) Burda, C.; Link, S.; El-Sayed, M. A. *Chem. Rev.* **2005**, *105*, 4.

Scheme 2. Comparison of Schematic Diagrams of the Electron Excitation−Relaxation Cycle for the Intraband Transition (a) within the 6sp Band and (b) for the 5d to 6sp Band Interband Transition with Particular Emphasis on Their Timescales

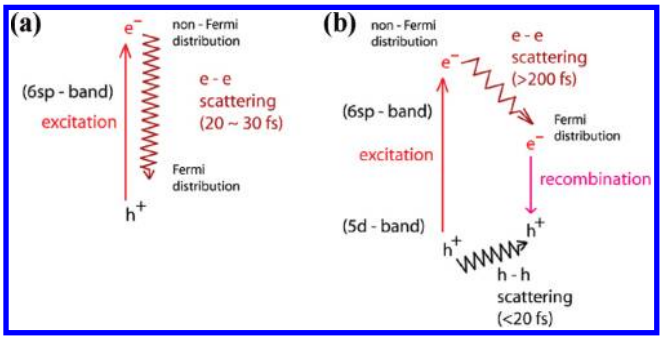

Scheme 2 gives an illustration of the excitation−relaxation cycles including the timescales for each step for the (a) intraband and (b) interband excitations.

The average energies (ΔE) for excitation at 532, 355, and 266 nm provide the e−e scattering time, τ_{e-e}, ranging from approximately 20−30 fs for 532 nm to >200 fs for 355 and 266 nm.[54] During the excitation−relaxation cycles of interband transitions (b), holes are created in the 5d band, which relax very quickly (<20 fs) through the hole−hole scattering and finally recombine nonradiatively with electrons from the lower-lying levels of the 6sp band.[54,55] This very fast recombination process generates holes in the 6sp band below the Fermi level with lifetimes on the order of >200 fs. During the nanosecond pulse duration, electrons in the 5d band can be excited again many times by incoming photons and the electron−hole (e−h) recombination between the 6sp band and 5d band occurs subsequent to the hole−hole (h−h) relaxation again and again. The repetition of this cycle brings about an appreciable reduction in electron concentration N around the Fermi level. Contrastingly, the reduction in N is practically absent for the intraband excitation (a) as a result of the fast relaxation of electrons within the 6sp band. The picture in Scheme 2 explains the remarkably reduced heat capacity observed for the interband excitation.

Previously, it was revealed by the femtosecond pump−probe spectroscopy that the transient bleaching of the plasmon band takes place, resulting in a temporal reduction in the absorption on subpicosecond timescales for the excitation of Au NPs with 30 nm diameter at both 400 and 600 nm.[56] In the present study, we employed the ground-state absorption cross section, C_{abs}, to calculate the values of Q at the three excitation wavelengths and assumed that such a transient reduction in the absorption intensity is negligible regardless of the excitation wavelength. However, this point was not confirmed in the present study because of experimental difficulty in measuring transient absorption spectra in the UV region.

For excitation by an ~200 fs laser pulse, a single excitation−relaxation cycle can take place, the timescale of which is much shorter than that of the electron−phonon (2.5 ps)[53] or phonon−phonon relaxation time (75−500 ps).[38,39] In other words, the reduction in N occurs only within the time duration of the laser pulse without affecting the thermalization process of the metal. Indeed, the previous femtosecond pump−probe studies revealed that the difference in interband excitation with respect to intraband excitation is absent for the electron−electron and electron−phonon relaxations.[56−58] Note, however, that laser heating with a nanosecond pulse makes no distinction between T_e (electron temperature) and T_l (lattice temperature) because of the exceedingly longer pulse duration of ~5 ns compared to the electron−electron and electron−phonon relaxation times. Obviously, in the nanosecond regime, the electron and lattice system are at thermal equilibrium,[59] $T_e = T_l = T$, through the energy exchange between the electron gas and the lattice with both temperatures rising during the pulse. Thus, the time-dependent temperature change can simply be expressed by the heat equation dependent on the particle temperature, T, and the specific heat capacity, c_p, as given in eq 7 under the condition that all the heat losses are negligible and there is a uniform temperature distribution within the NPs.[59]

$$\rho V c_p(T)\frac{\partial T}{\partial t} = C_{abs}^{\lambda} P \tag{7}$$

The solution for this differential equation was given in eqs 2a and 2b, which correctly reproduced the result of the 532 nm excitation. In contrast, femtosecond pulses with a much shorter duration than the electron−phonon relaxation time allows the differentiation of T_e and T_l. Here, electrons are excited during the femtosecond pulse followed by energy transfer to the lattice through electron−phonon coupling until thermal equilibrium is reached. This phenomenon is well described by the two-temperature model[60] (TTM) given in eqs 8a and 8b assuming no heat diffusion within the NPs with negligible energy losses.

$$c_e(T_e)\frac{\partial T_e}{\partial t} = -g(T_e - T_l) + Q(t)\rho \tag{8a}$$

$$c_l\frac{\partial T_l}{\partial t} = g(T_e - T_l) \tag{8b}$$

Here, g represents the electron−phonon coupling coefficient. It is most likely that we can directly observe the reduction in the value of c_e due to interband excitation by the use of a femtosecond pulsed laser. This may prove the validity of our present assumption. Great care must be taken with respect to the laser intensity in order not to bring about violent processes such as laser ablation and the photothermal effect. Such an experiment is now underway in our laboratory, and the results will be reported soon.

Conclusions

The present in situ spectroscopic measurement and TEM observation on nanosecond laser-induced reshaping and size reduction of Au nanoparticles have demonstrated a remarkably greater efficiency of the photothermal effect of interband excitation than that of intraband excitation. Previously, it was believed that the excitation of the surface plasmon resonance band is the most efficient way to induce heating resulting in the melting and fragmentation of Au NPs because of a distinctly large absorption

(54) Zhukov, V. P.; Aryasetiawan, F.; Chulkov, E. V.; Gurtubay, I. G.; Echenique, P. M. *Phys. Rev. B* **2001**, *64*, 195122.
(55) Dulkeith, E.; Niedereichholz, T.; Klar, T. A.; Feldmann, J. *Phys. Rev. B* **2004**, *70*, 205424.
(56) Ahmadi, T. S.; Logunov, S. L.; El-Sayed, M. A. *J. Phys. Chem.* **1996**, *100*, 8053.
(57) Hodak, J. H.; Martini, I.; Hartland, G. V. *J. Phys. Chem. B* **1998**, *102*, 6958.
(58) Perner, M; Bost, P.; Lemmer, U.; von Plessen, G.; Feldmann, J.; Becker, U.; Mennig, M.; Schmitt, M.; Schmidt, H. *Phys. Rev. Lett.* **1997**, *78*, 2192.
(59) Chichkov, B. N.; Momma, C.; Nolte, S.; Alvensleben, F.; Tünnermann, A. *Appl. Phys. A* **1996**, *63*, 109.
(60) Grua, P.; Morreeuw, J. P.; Bercegol, H.; Jonusauskas, G.; Vallée, F. *Phys. Rev. B* **2003**, *68*, 035424.

cross section. The greater photothermal efficiency due to the interband excitation at 266 nm is ascribed to the 60% decreased value of the specific heat capacity, c_p, compared to that of bulk gold. The excitation at 355 nm should provide an analogous value of c_p. In contrast, the value of c_p estimated for the excitation of the plasmon band at 532 nm was in good agreement with the literature value of bulk gold. We gave a semiquantitative explanation for the reduced c_p value as being due to the reduction in the electron concentration in the vicinity of the Fermi level through fast hole−hole relaxation followed by recombination and slow electron−electron relaxation in the conduction band resulting from the interband excitation. However, our explanation is still less satisfactory and needs further experimental proof. To overcome this limitation, pump−probe spectroscopy employing a nanosecond laser pump with a femtosecond laser probe may help to understand the excited energy-relaxation process due to the excitation at 266 nm, which may differ from that due to the excitation at 532 nm. Nevertheless, the present results shed new light on one of the fundamental properties of noble metal nanoparticles—the heat capacity that can be changed during UV photoexcitation. In addition, our finding implies that the heat capacity change has to be taken into serious consideration for the interband excitation of gold nanoparticles, which has not been considered in previous studies of the laser-induced size reduction. The specific heat capacity change can be applied to prepare new materials, for instance, nanoparticles with porous structures through the laser irradiation of alloys such as white gold, containing materials with differing interband and intraband excitation probabilities at a given laser wavelength.

Acknowledgment. Financial support by KAENHI (no. 21020025) on priority area Strong Photon-Molecule Coupling Field (no. 470) is gratefully acknowledged. A stimulating discussion with Dr. Takuro Tomita of The University of Tokushima is gratefully acknowledged. Mr. Minoru Tagami, Mr. Tomoyuki Ueki, and Dr. Yoji Makita are acknowledged for TEM photograph acquisition.

Supporting Information Available: Extinction spectra, TEM images, and size distribution of gold particles employed in this study. Remark on the estimation of absorbed laser energy by Au NPs. Simulated spectra of continuous size reduction based on the Mie theory. In situ spectra for the original 55 nm gold particles in aqueous solution. Remark on thermionic emission and the photoelectric effect. Method of estimating Q_{melt} and Q_{evap} to calculate the specific heat capacities. Remarks on in situ spectral measurements for the initial 20 nm Au NPs in aqueous solution. TEM and extinction spectroscopic observations of laser-induced size reduction of 20 nm Au NPs. Contribution of inter- and intraband components to the absorption spectra of 60 and 20 nm Au NPs and the Fermi distribution for bulk gold. ΔA versus laser fluence (mJ cm^{-2}) representation of the experimental data given in Figure 2. This material is available free of charge via the Internet at http://pubs.acs.org.